Sigma Overbounding using a Position Domain Method for the Local Area Augmentaion of GPS

JIYUN LEE
SAM PULLEN
PER ENGE, Fellow, IEEE
Stanford University

The local area augmentation system (LAAS) is a differential GPS navigation system being developed to support aircraft precision approach and landing navigation with guaranteed integrity and availability. While the system promises to support Category I operations, significant technical challenges are encountered in supporting Category II and III operations. The primary concern has been the need to guarantee compliance with stringent requirements for navigation availability. This paper describes how a position domain method (PDM) may be used to improve system availability by reducing the inflation factor for standard deviations of pseudo-range correction errors. Used in combination with the current range domain method (RDM), a 30% reduction in the inflation factor is achieved with the same safety standard. LAAS prototype testing verifies the utility of the PDM to enhance Category II/III user availability.

Manuscript received June 30, 2006; revised December 4, 2006 and March 25, 2008; released for publication June 16, 2008.

IEEE Log No. T-AES/45/4/935092.

Refereeing of this contribution was handled by M. Braasch.

This work was supported by the Federal Aviation Administration Satellite Navigation LAAS Program Office (AND-710).

Authors' current addresses: J. Lee, Dept. of Aerospace Engineering, Korea Advanced Institute of Science and Technology, Deajeon, Republic of Korea, Email: (jiyunlee@kaist.ac.kr); S. Pullen and P. Enge, Dept. of Aeronautics & Astronautics, Stanford University, Durand Bldg., Rm. 250, Stanford, CA 94305-4035.

I. INTRODUCTION

An aircraft navigation system must guarantee flight safety by assuring the position solution at a reliable level with protection bounds. The local area augmentation system (LAAS) is being developed as a ground-based augmentation of GPS by the Federal Aviation Administration (FAA). As such, navigation integrity is quantitatively appraised using the position bounds that assure an acceptable level of integrity risk. In this regard, aircraft compute the vertical protection level (VPL) and the horizontal protection level (HPL) as position error bounds using integrity data. These are then compared with the vertical alert limit (VAL) and the horizontal alert limit (HAL), respectively, to determine whether the system provides safety for each user.

One key integrity parameter used in the computation of these protection levels (PLs) is the standard deviation of pseudo-range correction errors (σ_{pr_gnd}) that is broadcast for each satellite approved by the LAAS ground facility (LGF) along with the correction message [1–3]. User integrity thus relies on these "sigmas." The prescribed methods for the generation of the PLs assume a zero-mean and normally distributed, fault-free error model for the broadcast pseudo-range corrections. However, the true errors are neither necessarily zero-mean nor Gaussian. The standard deviation of the correction error is further assumed to be equal to the broadcast value of σ_{pr_gnd}. If the broadcast error model does not overbound the true (unknown) error distribution, a serious threat to the aircraft may result. Thus, special care must be taken to validate these assumptions.

A great deal of prior work has been done to ensure that the zero-mean Gaussian distribution based on the broadcast σ_{pr_gnd} overbounds the true distribution, which may be non-Gaussian and non-zero-mean. There are two principal approaches. The first approach taken in LAAS is to transmit inflated values of the standard deviations which compensate for the uncertainty of the true error distribution. The main sources of statistical uncertainty are site installation errors due to the limited size of data and nonstationary error distributions caused by multipath variation. Pervan and Sayim [4] investigated the estimation error due to the finite sample sizes used to generate the model and error correlation across multiple reference receivers and derived the minimum acceptable inflation parameters for the value of the broadcast sigma. Their work implicitly assumed a zero-mean Gaussian error model associated with thermal noise and diffuse multipath. However, other error sources, such as ground reflection multipath and systematic reference receiver/antenna errors, may not be zero-mean Gaussian distributed. Shively and Braff [5] derived inflation factors to deal with

this non-Gaussian effect using a synthetic model of a Gaussian core and Laplacian tails. Rife [6] introduced a modified overbounding technique, called core overbounding. His Gaussian core with Gaussian sidelobe (GCGS) approach mitigates overconservatism associated with bounding heavy tails by providing an allowable envelope of tail distributions.

The second approach used in LAAS detects violations of the resulting overbound using the sigma monitor in failure events, where the true sigma exceeds the broadcast sigma or the true mean becomes substantially non-zero. Sources of unexpected anomalies in corrected pseudo-ranges can be multipath error increases due to varying environmental conditions, receiver noise error amplifications due to any natural system failure, or all other possible malfunctions. Lee [7] developed the two sigma monitor algorithms, direct estimation and cumulative sum (CUSUM) methods, and showed that real-time protection against sigma failures was achievable.

While the sigma overbounding techniques described above promise to support Category I operations, significant technical challenges are encountered in supporting Category II/III operations. This is due to the tightened VAL (a bound on maximum tolerable VPL) of 5.3 m and high availability requirements (0.999 or higher, depending on the airport). In addition, the maximum permissible integrity risk is on the order of 10^{-9} (i.e., the PLs must overbound the true position error, which is unknown in real time, with a probability of $1 - 10^{-9}$.) Thus, high levels of sigma inflation (with which the system may meet Category I requirements) cannot be tolerated for Category II/III approaches. This concern led to the application of a position domain method (PDM). Markin and Shively [8] originally introduced the concept of position domain monitoring in the mid-1990s as an alternative to range domain monitoring. The computed protection levels in the range domain may be conservative, since the range domain method requires a transformation from pseudo-range correction errors to position error estimates. In contrast, this alternative technique avoids the conservatism by performing a safety check directly in the position domain. An extended benefit from the PDM has been shown by Braff [9]. In this work, the method was found to be effective to reduce a conservatism that was applied to protect against the event that the pseudo-range correction error distribution was not modeled properly.

The PDM performs the integrity check by monitoring position solutions from combined sets of satellites [10]. In this concept, the PDM collects measurements with a remote receiver and derives position solutions by applying LGF corrections to all visible satellites approved by the LGF and all possible subsets of satellites. The position solutions are then compared to the known (surveyed) location of the PDM antenna, and errors exceeding detection thresholds are alerted. This method was considered an alternative to the range domain method (RDM), which monitors each pseudo-range measurement individually and approves each satellite for aircraft use. However, relying on only PDM turned out to be impractical due to limited data-link capacity and flexibility because it was thought that the PDM required generating every possible combination of satellites that may be used to compute the position solution and approving usable sets on a combination-by-combination basis. Thus, the current LGF is based on the RDM. However, given that an enhanced LGF architecture is required to meet Category II/III requirements, sigma overbounding using the PDM may be considered. This paper investigates how the PDM may be used to improve system availability by reducing the inflation factor for the standard deviation of pseudo-range correction errors and presents a method of sigma overbounding for Category II/III approaches. Section II introduces the PDM algorithm to compute position error estimates (the algorithm of monitoring is not described in this paper because it is irrelevant to the calibration of the inflation factor). Section III then discusses the characteristics of error distributions in the position domain. Section IV describes the unique, detailed approach to estimate $\sigma_{\text{pr\_gnd}}$ inflation factors and demonstrates that the PDM supports a smaller $\sigma_{\text{pr\_gnd}}$ inflation factor needed for Category II/III operations. Section V presents field-testing results showing improved system performance. Section VI summarizes the paper and suggests a direction for future research.

II. POSITION DOMAIN METHOD

PDM position solutions are computed using the approach required of LAAS airborne receivers—as specified in the LAAS Minimum Operational Performance Standards (MOPS) [3]—to emulate LAAS aircraft conditions as much as possible (the same method is used to obtain pseudouser position estimates and evaluate performance in Section V). In order to reduce errors in raw pseudo-range measurements for satellite n, ρ_n, we first apply the following carrier-smoothing filter [1, 3]. The smoothed pseudo-range ρ_s for satellite n at epoch k is

$$\rho_{s,n}(k) = \frac{1}{N_s}\rho_n(k) + \frac{N_s - 1}{N_s}(\rho_{s,n}(k-1) + \phi_n(k) - \phi_n(k-1)), \quad n = 1,2,\ldots,N \qquad (1)$$

where ϕ is the carrier phase measurement, and N_s is equal to 200 since this filter uses a time constant τ_s of

100 s and a sampling interval, T_s, of 0.5 s

$$N_s = \tau_s/T_s = 100/0.5 = 200. \tag{2}$$

Next we apply the set of LGF differential corrections to these carrier-smoothed code measurements [3]. The corrected pseudo-range measurements are

$$\rho_{c,n}(k) = \rho_{s,n}(k) - \rho_{\text{corr},n}(k-1) - R_{\rho_{\text{corr},n}}(k-1)\cdot T_s + TC(k) + c\cdot\Delta t_n(k) \tag{3}$$

where ρ_{corr} and $R_{\rho_{\text{corr}}}$ are the pseudo-range correction and the range rate correction from the LGF-approved message [3]. The variable TC is the tropospheric correction and is small enough to be neglected in this application. The parameter c represents the vacuum speed of light, and Δt_n is the satellite clock correction computed using clock parameters in subframe 1 of the GPS navigation message. Based on this set of differentially corrected measurements, we compute three-dimensional positions using a linearized, weighted least-squares estimation method. The linearized measurement model is

$$\underbrace{\rho_{c,n}(k) - \rho_{0,n}(k)}_{\Delta y} = G\underbrace{\begin{bmatrix}\delta x(k)\\ \delta y(k)\\ \delta z(k)\delta b(k)\end{bmatrix}}_{\Delta x} + \tilde{\varepsilon} \tag{4}$$

where Δx is the four dimensional position $(\delta x, \delta y, \delta z)$/clock bias (δb) deviation vector, Δy is an N-dimensional observation deviation vector containing the corrected pseudo-range measurements (ρ_c) minus the expected ranging values (ρ_0) based on the location of the PDM antenna and satellites, $\tilde{\varepsilon}$ is an N-dimensional vector containing the remaining errors in the corrected measurements, and G is the observation matrix consisting of N rows of line-of-sight vectors from each satellite to the PDM antenna, augmented by a "1" for the clock. Thus, the nth row of G corresponds to the nth satellite in view and can be written in terms of the azimuth angle (Az_n) and the elevation angle (El_n). This matrix is unitless and is defined as

$$G = \begin{bmatrix} -\cos El_1(k)\cos Az_1(k) & -\cos El_1(k)\sin Az_1(k) & -\sin El_1(k) & 1\\ -\cos El_2(k)\cos Az_2(k) & -\cos El_2(k)\sin Az_2(k) & -\sin El_2(k) & 1\\ \vdots & \vdots & \vdots & \vdots\\ -\cos El_N(k)\cos Az_N(k) & -\cos El_N(k)\sin Az_N(k) & -\sin El_N(k) & 1\end{bmatrix}. \tag{5}$$

We find the weighted least-squares solutions for the estimate of the states by

$$\Delta\hat{x} = S\cdot\Delta y, \qquad S \equiv (G^T W G)^{-1} G^T W \tag{6}$$

where S is the weighted least square projection matrix, and the inverse of the least-squares weighting matrix is

$$W^{-1} = \begin{bmatrix}\sigma^2_{PR,1} & 0 & \cdots & 0\\ 0 & \sigma^2_{PR,2} & \cdots & 0\\ \vdots & \vdots & \ddots & 0\\ 0 & 0 & 0 & \sigma^2_{PR,N}\end{bmatrix}. \tag{7}$$

Here, $\sigma_{PR,n}$ is the fault-free error model associated with satellite n:

$$\sigma^2_{PR,n} = \sigma^2_{\text{air},n} + \sigma^2_{\text{tropo},n} + \sigma^2_{\text{iono},n}. + \sigma^2_{\text{pr\_gnd},n}. \tag{8}$$

The airborne error σ_{air} is determined from the receiver noise estimate and the specified multipath model. The second and the third terms are introduced by the residual tropospheric and ionospheric errors, respectively. The ground error, $\sigma_{\text{pr\_gnd}}$, includes the ground station receiver noise and multipath error (see Appendix for details). Although the purpose of the PDM is to imitate aircraft operations, the PDM is still a ground-based system with ground-reflection multipath. Thus, we need to replace the airborne error sigma, σ_{air}, with the ground facility error sigma, $\sigma_{\text{pr\_gnd}}$. The choice of σ_{air} being equal to $\sigma_{\text{pr\_gnd}}$ is also made for a pseudouser as well as for the PDM receiver in Section V as a representative example. Comparing the position solutions $(\hat{x})$ with the known location of the PDM antenna (x_{surveyed}), we have the position error, χ, which is equivalent to $\Delta\hat{x}$ in (6):

$$\chi = \underbrace{\hat{x} - x_{\text{surveyed}}}_{\Delta\hat{x}}. \tag{9}$$

Here, the vertical component of χ in an East, North, up (ENU) coordinate system is the vertical position error, which is used to calibrate an inflation factor for the broadcast $\sigma_{\text{pr\_gnd}}$.

III. ERROR DISTRIBUTION IN POSITION DOMAIN

This section investigates how range domain error statistics are converted into position domain error statistics. The purpose here is to show that the error distribution has thinner tails than before the conversion, which is a key factor supporting a smaller sigma inflation factor and consequently improving navigation availability. From (6) and (9), the relationship between pseudo-range correction

errors and position errors is

$$\chi = S_1(\underbrace{\hat{\varepsilon}_1 - b_1}_{\Delta y_1}) + S_2(\underbrace{\hat{\varepsilon}_2 - b_2}_{\Delta y_2}) \cdots + S_N(\underbrace{\hat{\varepsilon}_N - b_N}_{\Delta y_N}) \tag{10}$$

where the pseudo-range correction errors for each satellite n (which is equivalent to Δy_n) can be expressed with the pseudo-range correction error with zero-mean $\hat{\varepsilon}_n$, and the mean bias of the correction errors b_n, for each satellite n. The position error, χ, is the sum of mean-biased correction errors, which are also weighted by the coefficients of the projection matrix (S_n). We now develop the connection between error distributions in the range and position domains. The probability density function (pdf) f of the sum of the weighted and mean-biased independent variables is the convolution of their respective scaled and mean-shifted pdfs f_r [11].

Based on this theorem and (10), the pdf of position errors $f(\chi)$ is

$$f(\chi) = \frac{1}{|S_1|} f_r\left(\frac{\hat{\varepsilon}_1 - b_1}{|S_1|}\right) * \frac{1}{|S_2|} f_r\left(\frac{\hat{\varepsilon}_2 - b_2}{|S_2|}\right) \cdots * \frac{1}{|S_N|} f_r\left(\frac{\hat{\varepsilon}_N - b_N}{|S_N|}\right). \tag{11}$$

Since $\hat{\varepsilon}_n$ is weighted by S_n and biased by b_n, the pdf of $\hat{\varepsilon}_n$ is scaled by S_n and shifted by b_n. We take convolutions of these pdfs to obtain $f(\chi)$.

An empirical model of pseudo-range correction errors ($\hat{\varepsilon}_n$) is developed as described in Section IVB. Using this model, shown in Fig. 1 as a dashed curve, we transform the error distribution in the range domain into the position domain. This is done by convolving the correction error pdfs, which are scaled and mean-shifted. The given weighting parameters S_n, and mean-bias parameter b_n, make the established position error model into a good representation of the experimental data (which is shown in Fig. 3). It is clear that the tails of the position error distribution (the solid curve in Fig. 1) are thinner than those of the individual correction error distributions (the dashed curve in Fig. 1). The thinner tails of the error distribution in the position domain are caused by the averaging effect of correction errors through the convolutions and common mode cancellation of correction errors. Note that the sum of weighting parameters is zero, $\sum_{n=1}^{N} S_n = 0$, and thus the common correction errors across ranging sources cancel out in (10).

IV. SIGMA INFLATION FACTOR ESTIMATION

As addressed in Section I, the true sigma may exceed the broadcast $\sigma_{\text{pr\_gnd}}$ due to the uncertainty of the true error distribution. The main sources of this uncertainty are mean and sigma estimation

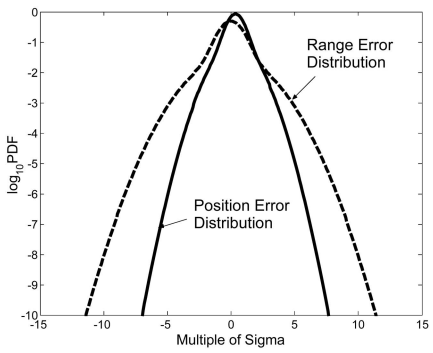

Fig. 1. Error distributions in position domain and in range domain.

error during site installation and nonstationary error distributions caused by environmental changes that affect multipath. Thus, the LGF needs to broadcast an inflated $\sigma_{\text{pr\_gnd}}$ such that the broadcast distribution overbounds all reasonable error distributions out to the probabilities assumed in the computation of the protection levels (PLs). The inflation factor, $f_{\text{inflation}}$, is defined as the ratio of the broadcast sigma to the theoretical sigma of a zero-mean and normally distributed correction-error model

$$f_{\text{inflation}} = \frac{\sigma_{\text{Broadcast}}}{\sigma_{\text{Theoretical}}}. \tag{12}$$

Although a great amount of work has been done regarding sigma inflation that accounts for each individual cause of the uncertainty [4, 5], an inflation factor that copes with all of the uncertainty sources at once has not yet been investigated.

This section introduces a comprehensive method of determining the inflation factor covering the following three sources of uncertainty: finite sample size, process mixing, and the limitation of sigma monitors. Section IVA considers the effect of sigma estimation error due to the limited number of samples. A basic assumption of the PL is that pseudo-range correction errors are zero-mean Gaussian distributed. However, in practice, the tails of the true error distribution may not be exactly Gaussian due to time-varying environmental conditions. In addition, even though we assume a stationary condition, mixing of Gaussian errors with different sigmas may cause the fattened tails. Section IVB deals with mixing of time-varying errors—such as ground reflection multipath—and mixing of different Gaussian distributions. An inflation factor is derived for the non-Gaussian tails in both the range and position domains. Section IVC then reviews the performance of the existing sigma monitors and provides a factor to overcome its limitations. Lastly, Section IVD presents a method to combine all factors and determine the inflation factors for the broadcast $\sigma_{\text{pr\_gnd}}$ in the range and position domains, respectively. These induced inflation factors are evaluated by computing PLs of a pseudouser in Section V.

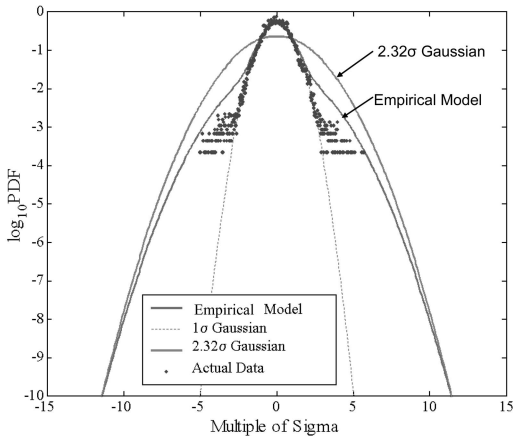

Fig. 2. Probability density function of normalized B-values (error distribution in range domain).

A. Finite Sample Size

In determining the broadcast sigma of the ground facility error, we must account for specific environmental conditions (antenna siting, gain patterns, and system configuration) of each LGF site. Even though these conditions are factored very accurately into sigma estimation and the environment is assumed to be stationary, the estimated sigma may have a statistical noise due to finite sample size. Previous research on this subject has been done by Pervan and Sayim [4]. They investigated the sensitivity of integrity risk to statistical uncertainties to which the correction error standard deviation and error correlation between multiple reference receivers are susceptible. Based on their work, the minimum acceptable inflation factor for the broadcast $\sigma_{\text{pr\_gnd}}$ is approximately 1.2 (see [4] for details).

B. Process Mixing

As noted above, the true LGF error distribution may change with time, as environment conditions vary. In addition, mixing of the time-varying errors—ground reflection multipath and systematic receiver/antenna errors—makes the characteristics of the error distribution complex. Even if stationary Gaussian error distributions are assumed, some degree of the mixture problem is expected. The standard deviation of the true error distribution varies as a function of the elevation angle of each satellite. If pseudo-range correction errors are normalized by the theoretical sigma which depends on the ranging source elevation angle but which is not perfect, this normalization mixes Gaussian distributions with different sigmas. The process mixing may result in non-Gaussian tails.

Fig. 2 shows the distribution of the LGF B-values collected by the Stanford Integrity Monitor Testbed (IMT)—an LGF prototype designed by Stanford University—for a period of 5 hr. The B-values are ground broadcast differences between the pseudo-range corrections derived from subsets of the multiple LGF reference receivers (typically 3 or 4). The precise mathematical formation of these B-values is defined in the LGF system specification [1]. Since the B-values represent pseudo-range correction differences across reference receivers—ideally, the pseudo-range corrections from all reference receivers should be the same for a given satellite—the B-values are best thought of as the estimates of pseudo-range correction errors under the hypothesis that a given reference receiver has failed. The B-values are normalized by their theoretical sigma which depends on the elevation angles, and those normalized B-values which are mixed over all elevations are used to configure the range error distribution. As addressed earlier, this mixing which results from the normalization may cause the fattened tails of the error distribution as mixing of time-varying errors does. In Fig. 2, we can clearly see that the correction error distribution (the dotted curve) has non-Gaussian tails (note that the scale of its vertical axis is logarithmic). Thus we should inflate the nominal 1σ Gaussian distribution (shown as the dashed curve) to overbound the error distribution with non-Gaussian tails. However, this error distribution modeled with experimental data is not sufficient to represent the true error distribution. In other words, a reliable estimation of the tail probabilities is impossible because their small magnitude (on the order of 10^{-10}) requires a huge sample size (greater than 10^{10}) that cannot be collected in a realistic time frame. Hence, the limited number of samples makes an empirical model necessary for estimating the error distribution. We use the following Gaussian-mixture distribution as the empirical model to represent the data better than the simplest and most common model of a single Gaussian pdf:

$$\begin{aligned} f_{GM} &= (1-\varepsilon)*N(\mu_0,\sigma_0)+\varepsilon*N(\mu_1,\sigma_1) \\ \varepsilon &= 0.15, \qquad \mu_0=\mu_1=0 \\ \sigma_0 &= 0.75, \qquad \sigma_1 = 1.82 \end{aligned} \tag{13}$$

where $N(\mu,\sigma)$ is a normal distribution with mean μ and sigma σ. Thus this function is the weighted sum of two normal distributions with one nominal sigma and one relatively large sigma. This model (the inner solid curve) shown in Fig. 2 well characterizes the actual distribution of Gaussian-core and non-Gaussian tails. Again, the nominal sigma should be inflated in order to cover the non-Gaussian tails of the actual distribution with a normal distribution. For Category I approaches, the tails need to be overbounded so that the probability of the error exceeding protection levels is less than or equal to 6×10^{-9} under the hypothesis of fault-free conditions (H0); for Category II/III approaches the required probability is 1.2×10^{-10}. To meet the integrity requirement, we need to inflate the

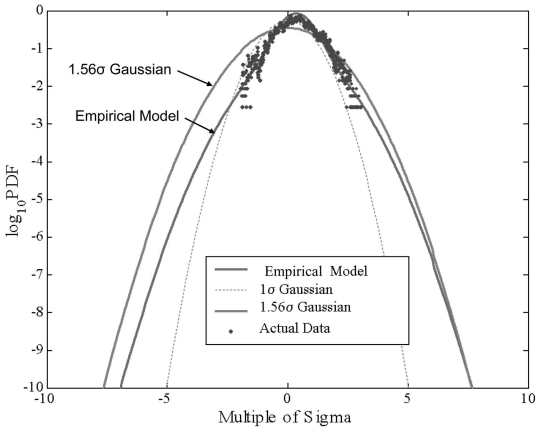

Fig. 3. Probability density function of normalized vertical position errors (error distribution in position domain).

sigma by a factor of 2.32 or greater. We can see that the 2.32σ Gaussian distribution (the outer solid curve) well overbounds the empirical model (the inner solid curve). As a result the minimum tolerable inflation factor is 2.32 if the LGF is based on range domain monitoring. Note that test statistics highly depend on system configurations; thus, this analysis should be conducted at each LGF site.

The result from Section III implies that the PDM allows us to reduce the inflation factor for broadcast $\sigma_{\text{pr\_gnd}}$ because its error density has thinner tails. Fig. 3 shows the distribution of vertical position errors, computed using the PDM algorithm for a period of 5 hr. The actual position error distribution (the dotted curve) is well characterized by the empirical model (the solid curve) also shown in Fig. 1. Note that this distribution has a shifted mean due to the mean biases of pseudo-range correction errors. Again since we assume a zero-mean normally distributed error model in the computation of PLs, we need to inflate the nominal sigma of a zero-mean Gaussian distribution to cover the non-Gaussian tails of the non-zero actual distribution. Thus, we inflate sigma to meet the H0 integrity risk allocation (1.2×10^{-10} for Category II/III [1]). Fig. 3 shows that the 1.56σ Gaussian distribution (the outer-solid curve) well overbounds the empirical model (the inner-solid curve). Consequently the minimum tolerable inflation factor to mitigate integrity risks due to process mixing is 1.56 if the LGF is based on the PDM. Again this analysis should be performed at each LGF site to account for different system configurations. Sigma overbounding has been shown in this paper using the pdfs in order to illustrate that empirical models well represent the actual distributions while demonstrating the overbounding. However, sigma overbounding must also be shown using cumulative distribution functions (cdfs) to ensure integrity as stated in [6]. Thus, we performed cdf overbounding for the cases shown in Figs. 2 and 3 and confirmed that the cdf overbounding was in a good agreement with the pdf overbounding.

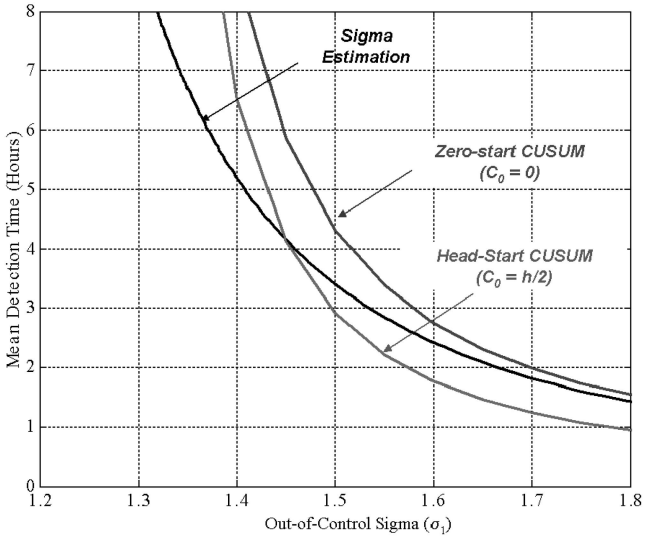

Fig. 4. Failure-state average run lengths for CUSUM and sigma estimation monitors.

C. Limitation of Sigma Monitors

The possibility of sigma violations exists because of not only the nominal sigma uncertainty but also unexpected anomalies. Thus, the sigma monitor is needed to provide necessary integrity in the event that the true sigma significantly exceeds the broadcast sigma. Lee [7] developed two different sigma-monitoring algorithms: the sigma estimation method and CUSUM method. The former detects relatively smaller violations faster, while the latter detects larger violations faster. These two sigma-monitoring algorithms together are able to detect any size of sigma violation that is hazardous to users. However, the current sigma monitor has a limitation on mean time-to-detect which must be overcome with an additional inflation factor. First, we derive the additional parameter assuming that the error distribution is Gaussian. Second, we assume a specific non-Gaussian error distribution and then derive the inflation factor.

1) *Gaussian Assumption on Error Model*: Let us review the performance of the sigma monitor implemented in the Stanford IMT (see [7] for details.) Fig. 4 shows the mean detection time for different sigma monitoring methods to detect certain failure-states—out-of-control sigmas (σ_1)—given the condition that the error distribution is Gaussian. The failure state is denoted as σ_1 (out-of-control sigma) which is the ratio of an actual sigma to a theoretical sigma

$$\sigma_1 = \frac{\sigma_{\text{Actual}}}{\sigma_{\text{Theoretical}}}. \tag{14}$$

We now turn our attention to the LGF requirements specified in [1] and reexamine the capability of this monitor. Based on the time-to-alert requirements, if the actual integrity risk is greater than the total allocation but the resulting risk increase

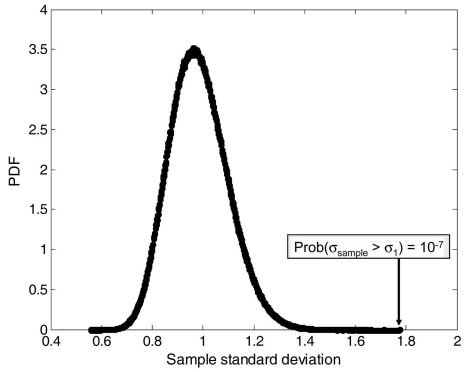

Fig. 5. Probability density function of sample standard deviation.

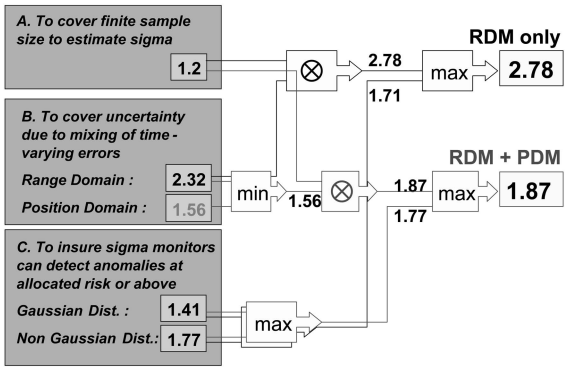

Fig. 6. Inflation factors for broadcast σ_{pr_gnd} with RDM only and RDM + PDM.

is minimal (i.e., is no greater than one order of magnitude), it is defined as "minimal-risk-increase." Since degraded performance due to such sigma failure is minimal according to the specification, we need not detect it immediately but instead within a day. Note that if sigma failure causes "nonminimal-risk-increase" (i.e., the integrity risk is increased by more than one order of magnitude from the total allocation), it should be detected within an hour. The limitation of the sigma monitor is now defined: Assuming that we can continuously collect data in one satellite pass for 5 hr on average, the minimum out-of-control sigma detectable within a day is 1.41. Out-of-control sigmas (σ_1) greater than the inflation factor ($f_{inflation}$) are categorized as "minimal-risk-increase" (i.e., the actual sigma exceeds the broadcast sigma), by definition of (12) and (14). If the inflation factor is less than 1.41, sigma violations with minimal risk—between the inflation factor and 1.41—cannot be alarmed within a day. Accordingly, in order to meet the LGF requirements, the inflation factor should be at least 1.41.

2) *Non-Gaussian Assumption on Error Model*: As pointed out in Section IVB, the error distribution may not be precisely Gaussian. Thus, we also need to consider the restriction of the sigma monitor given the assumption that the errors are non-Gaussian distributed. Results corresponding to Fig. 4 are generated using the non-Gaussain model described in (13). This model is an example used to represent the actual distribution. From this distribution we collect 90 independent samples to compute a sample standard deviation. Note that 90 is the number of independent samples that we can collect continuously in 5 hr, since 18 independent samples correspond to 1 hr (the interval between independent B-values is taken to be equal to 200 s, which is twice as long as the time constant of the carrier-smoothing filter [1, 7].) Repeating this process randomly, we then generate 10,000,000 sample sigmas. As a result, the pdf of a sample sigma is shown in Fig. 5. Based on the specified fault-free alarm rate, 10^{-7} (a sub-allocation of Category I continuity risk allowed per 15 s interval [1, 12]), the minimum out-of-control sigma detectable within 5 hr is now 1.77. Consequently, to protect this particular non-Gaussian error model, the inflation factor should be at least 1.77.

D. Total Inflation Factor

So far we have investigated three major sources of sigma uncertainty and derived an inflation factor for each source. The final step is to determine the total inflation factor for the broadcast σ_{pr_gnd} considering all conditions discussed in Sections IVA, IVB and IVC:

1) The theoretical (or preestimated) sigma is to be inflated by a factor of 1.2 to account for finite sample size (Section IVA).

2) The inflation factors to overbound the tails of the non-Gaussian distribution derived from IMT data are 2.32 in the range domain and 1.56 in the position domain (Section IVB).

3) The inflation factor should be at least 1.77 to overcome limitations of the existing sigma monitor (Section IVC).

In Fig. 6, we present the inflation factor determination method for the broadcast σ_{pr_gnd}. Since the conditions described in Sections IVA and IVB are independent, we multiply the two parameters (1.2 and 2.32) for the range domain case. The resulting factor (2.78) already exceeds what is required by the sigma monitor (which is 1.77) satisfying the third condition. Thus, the total inflation factor is 2.78 when the LGF is based on the RDM only. Using the same method, we obtain the total inflation factor for the position domain case. We multiply the two parameters (1.2 and 1.56) derived in Sections IVA and IVB, and then take the maximum of the resulting factor (1.87) and 1.77 derived in Section IVC. Note that among induced parameters to cope with each error source, only the second one—the inflation factor to cover process mixing—changes; the others remain the same in the position domain. The total inflation factor is 1.87 when a PDM is added to the current RDM (as addressed earlier, the LGF cannot rely solely on the

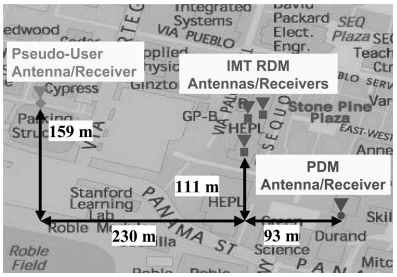

Fig. 7. Stanford LAAS performance test-bed IMT-PDM-user hardware configuration.

PDM due to limited data-link capacity and complexity and thus the LGF may augment the existing system by adding the PDM). These total inflation factors are used to compute vertical protection levels in the following section.

V. PERFORMANCE ANALYSIS

To demonstrate that the position domain method provides users with sharper confidence bounds due to the reduced inflation factor and consequently improves system availability, this section evaluates the system performance by computing a pseudouser's protection levels. The two postprocessing runs are conducted to compare performance: the first run using the augmented system with the position domain method and the second run with the current Stanford IMT (range domain monitoring only).

A. Performance Testbed Architecture

To evaluate whether the LGF can meet its integrity requirements, Stanford University researchers have developed an LGF prototype known as the Integrity Monitor Testbed (IMT) [13]. The LGF requires that redundant differential GPS reference receivers be able to detect and exclude failures of individual receivers. Fig. 7 shows the configuration of the three IMT antennas on the Stanford HEPL (Hansen Experimental Physics Laboratory) rooftop. The existing IMT antennas are connected to three NovAtel OEM-4 reference receivers which are connected to the IMT computer by a multiport serial board. The separations between these three NovAtel Pinwheel (survey grade) antennas are limited to 20–65 m by the size of the HEPL rooftop but are sufficiently separated to minimize the correlations between individual reference receiver multipath errors (this has been demonstrated by previous work) [13, 14]. Each receiver can track as many as 12 satellites simultaneously. Each receiver samples GPS signals every 0.5 s and provides receiver measurement packets, which contain pseudo-range measurements, carrier-phase measurements, and navigation messages. These GPS measurements are fed into the IMT processor for further calculations.

A prototype of PDM has been applied to the existing Stanford IMT as shown in Fig. 7. We use the Stanford WAAS Reference Station antenna (located on the Stanford Durand Building) for the PDM antenna, which is separated by approximately 145 m from the IMT antennas. In order to test the capability of meeting the high availability requirement for Category II/III precision approaches, we have tested LAAS augmented with the PDM by installing a static "pseudouser" antenna/receiver on top of the nearby parking structure. The NovAtel Pinwheel antenna ("pseudouser" antenna) and the center of the IMT are approximately 230 m apart, and the distance between the pseudouser antenna and the PDM antenna is approximately 360 m. The NovAtel OEM-4 receivers connected to the PDM antenna and the "pseudouser" antenna collect pseudo-range measurements, carrier-phase measurements, and navigation messages of GPS satellites ("pseudouser," PDM, and IMT receivers are set up to collect measurements simultaneously). The measurements are postprocessed in a single computer where the PDM algorithm is developed and tested.

B. Experimental Result

In order to evaluate system performance, we first compute position errors, which are obtained by comparing the surveyed location of the pseudouser's antenna to position solutions. Pseudouser position solutions are computed in the manner required of the LAAS airborne receivers to mirror LAAS aircraft operations to the degree possible (the detailed algorithm is specified in the RTCA LAAS MOPS [3] and also in Section II). In this analysis, accuracy designator C (AD-C) is applied to the pseudo-range error model [15], as it corresponds to the hardware installation for Category II/III (see Appendix). Second, we compute protection levels through which the final quantitative appraisal of the navigation performance is realized. The VPL under the hypothesis of fault-free conditions (H0) is

$$\begin{aligned} \mathrm{VPL}_{\mathrm{H0}} &= K_{\mathrm{ffmd}}\sigma_{\mathrm{VerticalPositionError}} \\ &= K_{\mathrm{ffmd}}\sqrt{\sum_{n=1}^{N} S_{\mathrm{vertical},n}^2\sigma_{PR,n}^2} \end{aligned} \tag{15}$$

where $\sigma_{\mathrm{VerticalPositionError}}$ is the standard deviation of vertical position errors, K_{ffmd} is a specified multiplier that determines the probability of fault-free missed detections (i.e., this multiplier is the quantile of a unit Gaussian distribution corresponding to 10^{-9} for Category II/III operations and is equal to 6.441 when the number of ground reference receivers is three) [3], $S_{\mathrm{vertical},n}$ is the projection of the local

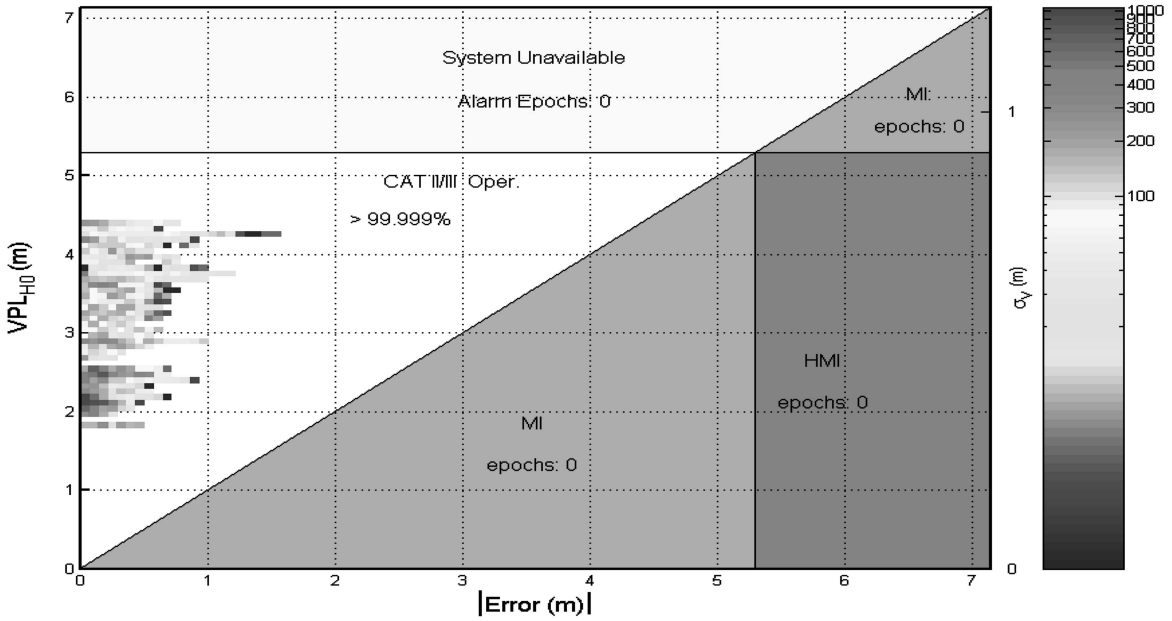

Fig. 8. System performance in vertical direction with RDM and PDM.

vertical component for the nth ranging source, and $\sigma_{PR,n}$ is the fault-free error model associated with satellite n. Since the vertical direction is the most stringent one and errors in this direction are generally worse than those in the lateral direction, we only pay attention to the vertical direction. From (8) and by applying the inflation factor, $f_{\text{inflation}}$, to the broadcast $\sigma_{\text{pr\_gnd}}$ to meet the integrity requirement (explained in Section IV), (15) can be expressed as

$$\text{VPL}_{\text{H0}} = K_{\text{ffmd}} \sqrt{\sum_{n=1}^{N} S_{\text{vertical},n}^2 \cdot [\sigma_{\text{air},n}^2 + \sigma_{\text{tropo},n}^2 + \sigma_{\text{iono},n}^2 + (f_{\text{inflation}} \cdot \sigma_{\text{pr\_gnd},n})^2]}. \tag{16}$$

We now proceed to verify that the inflation factor derived from the PDM can be substituted into (16). From (8) and (15), the standard deviation of the vertical position errors is

$$\sigma_{\text{VerticalPositionError}} = \sqrt{\sum_{n=1}^{N} S_{\text{vertical},n}^2 [\sigma_{\text{air},n}^2 + \sigma_{\text{tropo},n}^2 + \sigma_{\text{iono},n}^2 + \sigma_{\text{pr\_gnd},n}^2]}. \tag{17}$$

Because the PDM receiver is located on the ground, we replace the airborne error sigma σ_{air} with the ground facility error sigma $\sigma_{\text{pr\_gnd}}$. Here $\sigma_{\text{air},n} = \sqrt{3}\sigma_{\text{pr\_gnd},n}$ since $\sigma_{\text{pr\_gnd},n}$ is set based on three reference receivers (see Appendix subsection A). Then (17) becomes

$$\sigma_{\text{VerticalPositionError}} = \sqrt{\sum_{n=1}^{N} S_{\text{vertical},n}^2 \cdot [3\sigma_{\text{pr\_gnd},n}^2 + \sigma_{\text{tropo},n}^2 + \sigma_{\text{iono},n}^2 + \sigma_{\text{pr\_gnd},n}^2]}. \tag{18}$$

We also use the fact that $\sigma_{\text{tropo},n}$ and $\sigma_{\text{iono},n}$ are negligible because of the short distance (approximately 145 m) between the IMT and PDM. When (18) is multiplied by the inflation factor,

$$f_{\text{inflation}} \cdot \sigma_{\text{VerticalPositionError}} = \sqrt{\sum_{n=1}^{N} S_{\text{vertical},n}^2 \cdot 4(f_{\text{inflation}} \cdot \sigma_{\text{pr\_gnd},n})^2}. \tag{19}$$

This indicates that we can directly apply the inflation factor derived using the position domain error statistics to the broadcast $\sigma_{\text{pr\_gnd}}$ in (16).

Fig. 8 shows the performance of the PDM-augmented system. For the purpose of comparison, we also produce the performance results with the RDM only and plot them in Fig. 9. Horizontal axes indicate the absolute value of vertical position errors (|VPE|), while VPLs are plotted in the vertical axes. Each bin represents the number of occurrences of a specific pair (error, protection level). The |VPE|s are always less than 2 m, which means that both types of LGF systems meet the accuracy requirement for Category II/III approaches. Integrity risk is defined as the probability that the position error exceeds the alert limit and no navigation system alert occurs within the time-to-alarm. The event

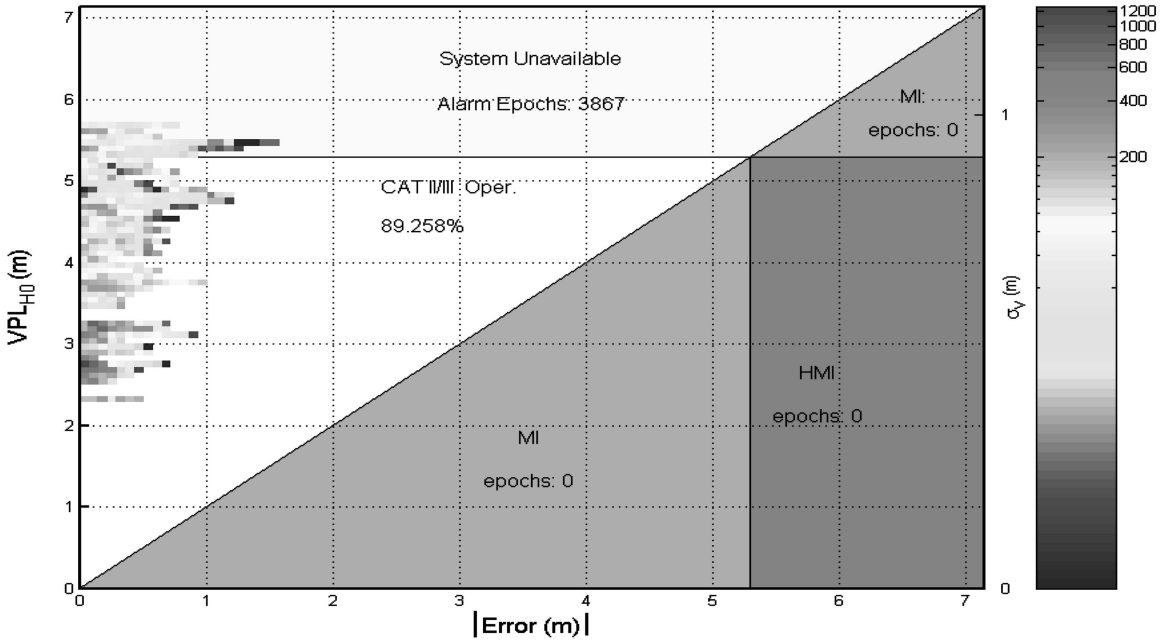

Fig. 9. System performance in vertical direction with RDM only.

with VPL less than the VAL but error greater than the VAL—which leads to hazardously misleading information (HMI), indicates a violation of integrity. In both plots, the errors are always less than the VPL and also VAL; thus, no points constitute integrity failures.

Now we turn our attention to LAAS availability, which is defined as the fraction of time for which the system is providing position fixes to the specified level of accuracy, integrity and continuity. If computed PLs exceed the alert limit, then the system no longer meets the integrity requirement and thus loses availability. The VAL for Category II/III precision approaches (indicated with horizontal and vertical lines in Figs. 8 and 9) 5.3 m based on the RTCA LAAS MASPS [16]. Without the PDM (and given the condition that available satellites in view are more than five), the system availability achieved in this analysis is only 89.258%, as shown in Fig. 9. Thus the RDM alone cannot meet the availability requirement of Category II/III approaches, which is 99.999%. In contrast, we can see in Fig. 8 that the system augmented with the PDM maintains the availability of 99.999% or greater in vertical positioning (when the same GPS constellation is provided as in the RDM only case). If we consider a relaxed VAL of 10 m based on the most recent LAAS MASPS update, it appears from Fig. 9 that the RDM would have been good enough for the data presented. However, in this assessment we computed the availability over only a period of 5 hr instead of a full day of geometries, and the GPS constellations with satellite outages were not considered. Also note that significantly less ideal sites may exist where the benefits of the PDM in addition to the RDM might make the difference between acceptable and unacceptable availability. Although further work is needed to better estimate the availability with the PDM, it is clear that the PDM augmentation helps meet the high Category II/III availability requirements (or provide that tool for future LAAS systems, should it ever be needed) by supporting a smaller inflation factor ($f_{\text{inflation}}$ = 1.87 versus 2.78)—inserted in (16) to compute VPLs—and consequently providing sharp protection bounds.

VI. CONCLUSIONS

This paper demonstrated that the PDM improves the performance of the existing Category I LGF, which is based on the RDM. We found that the performance achieved by adding the PDM aids significantly in meeting the stringent availability requirements of Category II/III operations. This improvement is possible because the PDM supports a lower inflation factor for the broadcast $\sigma_{\text{pr\_gnd}}$ (i.e., there is no availability penalty due to the conservative inflation factor as there is with the RDM). The paper also provides a comprehensive method for determining the sigma inflation factor. The derived inflation factor includes partial parameters for all sources of the sigma uncertainty and for the limitation of the current sigma monitor. The empirical performance tests showed that the system augmented with the PDM provides a 25% reduction in VPL with the same safety standard and enhances user availability.

Test statistics for determining a sigma inflation factor depend heavily on antenna sites, gain patterns,

and the nearby environment. Thus, the inflation factor derived in this paper is not applicable to all situations. For example, a challenging airport site or a ground-based system with upgraded hardware would require different inflation factors. Future research should focus on constructing more PDM test statistics with datasets collected from different environmental conditions for longer periods of time. Analyzing these statistics may help better evaluate PDM performance.

ACKNOWLEDGMENTS

The constructive comments and advice regarding this work provided by many other people in the Stanford GPS research group are greatly appreciated.

APPENDIX. LAAS ERROR MODELS

This Appendix describes the LAAS Accuracy Models used in this paper. These models are required to compute protection levels. Working Group-4 of RTCA Special Committee 159 developed standard error models for LAAS differential processing [1]. The standard GPS interference environmental conditions—the RF interference environment at and around L-band frequencies for LAAS airborne receivers—assumed in the models are defined in Appendix D of the LAAS MOPS (RTCA/DO-253A [3]). This group defined ground accuracy designators (GADs) that reflect different performance levels of GPS receiver technologies [15]. GAD-A represents a level of performance achievable with early and low-cost LAAS installations using a standard correlator receiver and a single-aperture antenna. GAD-C was defined to characterize the performance realizable with a narrow correlator receiver and a multipath limiting antenna (MLA). GAD-C performance is expected to be able to support LAAS CAT II/III precision approaches. GAD-B represents an intermediate level of performance between GAD-A and GAD-C. The performance of GAD-B is attainable with advanced receiver technologies similar to GAD-C but with a single-aperture antenna instead of an MLA.

A. Model of Ground Facility Error

The ground facility error sigma $\sigma_{\text{pr\_gnd}}$, which is broadcast to users by the LGF is a critical factor for airborne users to compute their position and integrity PLs. This error standard deviation for each ranging source should account for all equipment and environmental effects, including receiver noise, local interference, and ground station multipath. The standard deviation of the ground facility error is [1]

$$\sigma_{\text{pr\_gnd},n}(k) = \sqrt{\frac{(a_0 + a_1 e^{-\theta_n(k)/\theta_0})^2}{M_n(k)} + (a_2)^2} \quad (20)$$

where M is the number of reference receivers that are averaged to obtain a differential correction, θ_n is the nth ranging source elevation angle, and a_0, a_1, a_2 and θ_0 for the applicable GADs are defined in Table I.

TABLE I
Ground Facility Error Allocation Model

Ground Accuracy Designator		a_0 meters	a_1 meters	a_2 meters	θ_0 deg
GAD-A		0.50	1.65	0.08	14.3
GAD-B		0.16	1.07	0.08	15.5
GAD-C	$\theta_n \geq 35°$	0.15	0.84	0.04	15.5
	$\theta_n < 35°$	0.24	0	0.04	—

B. Model of Airborne Pseudo-range Performance

To define airborne pseudo-range error allocations for carrier-smoothed code processing, we consider two components. First, σ_{noise} is the error due to wideband noise and interference including receiver noise, thermal noise, inter-channel biases, extrapolation, and processing errors, and is modeled as

$$\sigma_{\text{noise},n} = a_0 + a_1 e^{-\theta_n/\theta_c}, \qquad 5° \leq \theta_n \leq 90° \quad (21)$$

where θ_n is the nth ranging source elevation angle, and a_0, a_1 and θ_c for the applicable airborne accuracy designator (AAD) are defined in [15]. The AADs were defined to reflect different performance levels of GPS receiver technologies. Second, $\sigma_{\text{multipath}}$ is the error due to airframe multipath and is described by the distribution, $N(0, \sigma^2_{\text{multipath}})$ where

$$\sigma_{\text{multipath},n} = 0.13 + 0.53 e^{-\theta_n/10°}. \quad (22)$$

The overall airborne accuracy model is computed as follows:

$$\sigma_{\text{air},n} = \sqrt{\sigma^2_{\text{noise},n} + \sigma^2_{\text{multipath},n}}. \quad (23)$$

C. Model of Tropospheric Residual Uncertainty

The standard deviation of the post tropospheric correction error is defined as [3]

$$\sigma_{\text{tropo},n} = \sigma_N h_0 \frac{10^{-6}}{\sqrt{0.002 + \sin^2(\theta_n)}}(1 - e^{-\Delta h/h_0}) \quad (24)$$

where σ_N is the refractivity uncertainty, h_0 is the tropospheric scale height from the LAAS type 2 message, Δh is the height of the aircraft above the LAAS reference point, and θ_n is the elevation angle of satellite n.

D. Model of Ionospheric Residual Uncertainty

Ionospheric temporal and spatial decorrelation can lead to differential LAAS user range errors.

The uncertainty of this residual ionospheric error is defined as [3]

$$\sigma_{\text{iono}} = F_{pp} \times \sigma_{\text{vert\_iono\_gradient}} \times (X_{\text{air}} + 2 \times \tau \times \nu_{\text{air}}) \tag{25}$$

where F_{pp} is the vertical-to-slant obliquity factor for a given satellite, $\sigma_{\text{vert\_iono\_gradient}}$ is the standard deviation of a normal distribution associated with the residual ionospheric uncertainty due to spatial decorrelation (a parameter provided by the ground subsystem in the LAAS type 2 message), X_{air} is the distance (slant range) between the aircraft and the LAAS reference point, τ is the time constant of the smoothing filter (100 s), and ν_{air} is the horizontal speed of the aircraft.

REFERENCES

[1] FAA
Specification: Performance Type One Local Area Augmentation System Ground Facility.
FAA, Washington, D.C., FAA-E-2937A, Apr. 17, 2002.

[2] FAA
Specification: Category I Local Area Augmentation System Non-Federal Ground Facility.
FAA, Washington, D.C., FAA/AND710-2937, May 31, 2001.

[3] RTCA
Minimum Operational Performance Standards for GPS Local Area Augmentation System Airborne Equipment.
RTCA, Washington, D.C., RTCA SC-159 WG-4A, DO-253A, Nov. 28, 2001.

[4] Pervan, B., and Sayim, I.
Sigma inflation for the local area augmentation of GPS.
IEEE Transactions on Aerospace and Electronic Systems, **37**, 4 (Oct. 2001), 1301–1311.

[5] Shively, C., and Braff, R.
An overbound concept for pseudorange error from the LAAS ground facility.
Proceedings of IAIN World Congress/ION 56th Annual Meeting, San Diego, CA, June 26–28, 2000, 661–671.

[6] Rife, J.
Core overbounding and its implications for LAAS integrity.
Proceedings of ION GNSS 2004, Long Beach, CA, Sept. 21–24, 2004, 2810–2821.

[7] Lee, J., Pullen, S., Xie, G., and Enge, P.
LAAS sigma monitor analysis and failure-test verification.
Proceedings of ION NTM 2001, Albuquerque, NM, June 11–13, 2001, 694–704.

[8] Markin, K., and Shively, C.
A position-domain method for ensuring integrity of local area differential GPS (LDGPS).
Proceedings of ION Annual Meeting, Colorado Springs, CO, June 5–7 1995, 369–380.

[9] Braff, R.
A method for LAAS fault-free error overbounding using a position domain monitor.
Proceedings of ION National Technical Meeting, Anaheim, CA, Jan. 22–24 2003, 326–388.

[10] Braff, R.
Position domain monitor (PDM) performance analysis for CAT III.
MITRE/CAASD, McLean, VA, Oct. 1, 2002.

[11] Ziemer, R. E.
Elements of Engineering Probability & Statistics (International ed.).
Upper Saddle River, NJ: Prentice-Hall, 1997.

[12] Pullen, S., Luo, M., Pervan, B., and Enge, P.
The use of CUSUMs to validate protection level overbounds for ground based and space based augmentations systems.
Proceedings of ISPA 2000, Munich, Germany, July 18–20, 2000, 355–371.

[13] Luo, M., Pullen, S., Zhang, J., Gleason, S., and Xie, G.
Development and testing of the Stanford LAAS ground facility prototype.
Proceedings of ION NTM, Anaheim, CA, Jan. 26–28, 2000, 210–219.

[14] Luo, M., and Pullen, S.
LAAS Reference Receiver Correlation Analysis.
Stanford University, Feb. 17, 1999.

[15] McGraw, G., Murphy, T., Brenner, M., and Pullen, S.
Development of the LAAS accuracy models.
Proceedings of ION GPS, Salt Lake City, UT, Sept. 19–22, 2000, 1212–1223.

[16] RTCA
Minimum Aviation System Performance Standards for the Local Area Augmentation System (LAAS).
RTCA, Washington D.C., RTCA SC-159 WG-4A, DO-245, Sept. 1998.

Jiyun Lee received the B.S. degree in astronomy from Yonsei University, Seoul, South Korea in 1997, the M.S. degree in aerospace engineering and science from the University of Colorado, Boulder, in 1999, and the M.S. and Ph.D. degrees in aeronautics and astronautics from Stanford University, Stanford, CA, in 2001 and 2005, respectively.

She is currently an assistant professor in the Mechanical Aerospace and Systems Engineering School at Korea Advanced Institute of Science and Technology. She is also a principal systems engineer at AMTI, Inc., and a consulting assistant professor at Stanford University. From 2007–2008, she worked at SiRF Technology, Inc. as a senior GPS systems engineer. She has been active in the Institute of Navigation (ION), serving as session cochair and track chair. She has received the ION Student Award and the Best Presentation Award for her work.

Sam Pullen received the Ph.D. in aeronautics and astronautics from Stanford University, Stanford, CA, in 1996.

He is a senior research engineer at Stanford, where he is the manager of the Local Area Augmentation System (LAAS) research effort. He supported the FAA in developing LAAS and WAAS system concepts, technical requirements, integrity algorithms, and performance models. He and his group have developed a LAAS ground facility prototype that utilizes innovative algorithms for detection, exclusion, and recovery of system failures. He is now developing ionosphere-anomaly-mitigation approaches for LAAS as well as improved system architectures and algorithms for the next phase of LAAS to support Category III precision landings.

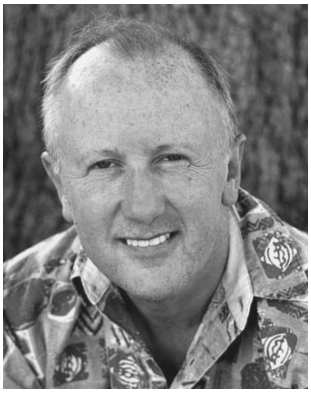

Per Enge (S'78—M'82) is the Kleiner-Perkins, Mayfield, Sequoia Capital Professor in the School of Engineering at Stanford University. He is also the Director of the GPS Research Laboratory, which pioneers satellite-based navigation systems for aviation and maritime use. Two of these systems are in widespread use today. Medium frequency beacons are used worldwide to broadcast differential GPS corrections to some 1.5 million, mostly marine, users. The first satellite-based augmentation system came online for aviation in the United States in July of 2003, and similar systems are being developed in Europe, Japan and India.

Dr. Enge has received the Kepler, Thurlow and Burka Awards for his work. He is also a member of the National Academy of Engineering and a Fellow of the ION.